ALMA and GMRT Constraints on the Off-axis Gamma-Ray Burst 170817A from the Binary Neutron Star Merger GW170817

S. Kim[1,2], S. Schulze[3], L. Resmi[4], J. González-López[1], A. B. Higgins[5], C. H. Ishwara-Chandra[6], F. E. Bauer[1,7,8],
I. de Gregorio-Monsalvo[9,10], M. De Pasquale[11], A. de Ugarte Postigo[12], D. A. Kann[12], S. Martín[9,10], S. R. Oates[13],
R. L. C. Starling[5], N. R. Tanvir[5], J. Buchner[1,7], S. Campana[14], Z. Cano[12], S. Covino[14], A. S. Fruchter[15], J. P. U. Fynbo[16],
D. H. Hartmann[17], J. Hjorth[18], P. Jakobsson[19], A. J. Levan[13], D. Malesani[18], M. J. Michałowski[20], B. Milvang-Jensen[18],
K. Misra[21], P. T. O'Brien[5], R. Sánchez-Ramírez[22], C. C. Thöne[12], D. J. Watson[16], and K. Wiersema[13]

[1] Instituto de Astrofísica and Centro de Astroingeniería, Facultad de Física, Pontificia Universidad Católica de Chile, Casilla 306, Santiago 22, Chile
skim@astro.puc.cl
[2] Max-Planck-Institut für Astronomie Königstuhl 17 D-69117 Heidelberg, Germany
[3] Department of Particle Physics and Astrophysics, Weizmann Institute of Science, Rehovot 761000, Israel; steve.schulze@weizmann.ac.il
[4] Indian Institute of Space Science & Technology, Trivandrum 695547, India; l.resmi@iist.ac.in
[5] Department of Physics and Astronomy, University of Leicester, University Road, Leicester LE1 7RH, UK
[6] National Center for Radio Astrophysics, Pune 411007, India
[7] Millennium Institute of Astrophysics (MAS), Nuncio Monseñor Sótero Sanz 100, Providencia, Santiago, Chile
[8] Space Science Institute, 4750 Walnut Street, Suite 205, Boulder, CO 80301, USA
[9] European Southern Observatory, Alonso de Córdova 3107, Vitacura, Santiago 763-0355, Chile
[10] Joint ALMA Observatory, Alonso de Córdova 3107, Vitacura, Santiago 763-0355, Chile
[11] Department of Astronomy and Space Sciences, Istanbul University, 34119 Beyazıt, Istanbul, Turkey
[12] Instituto de Astrofísica de Andalucía (IAA-CSIC), Glorieta de la Astronomía, s/n, E-18008, Granada, Spain
[13] Department of Physics, University of Warwick, Coventry CV4 7AL, UK
[14] INAF—Osservatorio astronomico di Brera, Via E. Bianchi 46, I-23807, Merate (LC), Italy
[15] Space Telescope Science Institute, 3700 San Martin Drive, Baltimore, MD 21218, USA
[16] Niels Bohr Institute, University of Copenhagen, Juliane Maries Vej 30, DK-2100 Copenhagen Ø, Denmark
[17] Department of Physics and Astronomy, Clemson University, Clemson, SC 29634-0978, USA
[18] Dark Cosmology Centre, Niels Bohr Institute, University of Copenhagen, Juliane Maries Vej 30, DK-2100 Copenhagen Ø, Denmark
[19] Centre for Astrophysics and Cosmology, Science Institute, University of Iceland, Dunhagi 5, 107 Reykjavík, Iceland
[20] Astronomical Observatory Institute, Faculty of Physics, Adam Mickiewicz University, ul. Słoneczna 36, 60-286 Poznań, Poland
[21] Aryabhatta Research Institute of observational sciencES (ARIES), Manora Peak, Nainital 263 001, India
[22] INAF, Istituto Astrofisica e Planetologia Spaziali, Via Fosso del Cavaliere 100, I-00133 Roma, Italy

Abstract

Binary neutron-star mergers (BNSMs) are among the most readily detectable gravitational-wave (GW) sources with the Laser Interferometer Gravitational-wave Observatory (LIGO). They are also thought to produce short γ-ray bursts (SGRBs) and kilonovae that are powered by r-process nuclei. Detecting these phenomena simultaneously would provide an unprecedented view of the physics during and after the merger of two compact objects. Such a Rosetta Stone event was detected by LIGO/Virgo on 2017 August 17 at a distance of $\sim$44 Mpc. We monitored the position of the BNSM with Atacama Large Millimeter/submillimeter Array (ALMA) at 338.5 GHz and the Giant Metrewave Radio Telescope (GMRT) at 1.4 GHz, from 1.4 to 44 days after the merger. Our observations rule out any afterglow more luminous than 3×10^{26} erg s^{-1} Hz^{-1} in these bands, probing >2–4 dex fainter than previous SGRB limits. We match these limits, in conjunction with public data announcing the appearance of X-ray and radio emission in the weeks after the GW event, to templates of off-axis afterglows. Our broadband modeling suggests that GW170817 was accompanied by an SGRB and that the γ-ray burst (GRB) jet, powered by $E_{\rm AG,iso} \sim 10^{50}$ erg, had a half-opening angle of $\sim$20°, and was misaligned by $\sim$41° from our line of sight. The data are also consistent with a more collimated jet: $E_{\rm AG,iso} \sim 10^{51}$ erg, $\theta_{1/2,\rm jet} \sim 5$°, $\theta_{\rm obs} \sim 17$°. This is the most conclusive detection of an off-axis GRB afterglow and the first associated with a BNSM-GW event to date. We use the viewing angle estimates to infer the initial bulk Lorentz factor and true energy release of the burst.

Key words: gamma-ray burst: individual (GRB 170817A) – gravitational waves

1. Introduction

The existence of gravitational waves (GWs) was predicted in 1916 (Einstein 1916, 1918), but it took almost a century to directly observe them (Abbott et al. 2016). A type of GW signal readily detectable with the Laser Interferometer Gravitational-wave Observatory (LIGO) is linked to the coalescence of two neutron stars (Abadie et al. 2010). This class of object is also thought to be the progenitor of short γ-ray bursts (SGRBs; duration $\lesssim$2 s; Eichler et al. 1989; Nakar 2007; Berger 2014). In addition, the temperatures and densities in the debris of the merger are thought to be high enough to also produce radioactive nuclei through rapid neutron capture. Their decays could give rise to faint supernova-like transients, called kilonovae (KNe; e.g., Li & Paczyński 1998; Rosswog 2005; Kasen et al. 2013; for a review see also Metzger 2017). Observational evidence for a KN was found in the near-infrared (near-IR) photometry of SGRB 130603B (Tanvir et al. 2013) and possibly in optical photometry of GRBs 050709 and 060614 (Jin et al. 2015, 2016). However, without a spectrum, the conjecture that SGRBs are accompanied by KNe, and therefore that SGRBs are connected with binary neutron-star mergers (BNSMs), is not free of ambiguity.

On 2017 August 17 at 12:41:04 UTC, the joint LIGO and Virgo observing run detected a BNSM at 40^{+8}_{-14} Mpc within an area of 28 deg^2 projected on the sky (Abbott et al. 2017b). The precise distance and localization gave the follow-up with optical wide-field imagers a flying start (for a comprehensive review see Abbott et al. 2017a). Coulter et al. (2017a) targeted galaxies at this distance and detected a new object, SSS17a (IAU identification: AT2017gfo; Coulter et al. 2017b), at $\alpha_{J2000} = 13^h09^m48^s.09$, $\delta_{J2000} = -23°22'53''.3$; $10''.3$ from NGC 4993 at 43.9 Mpc ($z = 0.00984$; Levan et al. 2017; for a detailed discussion see also Hjorth et al. 2017).[23] This discovery was confirmed by several teams including Allam et al. (2017), Melandri et al. (2017), Tanvir & Levan (2017a), and Yang et al. (2017). The transient rapidly faded in the optical, but showed a much slower evolution in the near-IR (Tanvir et al. 2017b). Spectra of AT2017gfo revealed very broad absorption features, due to relativistic expansion velocities (Pian et al. 2017; Smartt et al. 2017; Tanvir et al. 2017b), similar to those expected for KNe (Kasen et al. 2013; Tanaka et al. 2014). Such features are unlike any known for supernova spectra and strongly argued for a connection between AT2017gfo and GW170817 (Siebert et al. 2017).

The Gamma-ray Burst Monitor (GBM) detector aboard the γ-ray satellite *Fermi* (Blackburn et al. 2017; Goldstein et al. 2017a, 2017b; von Kienlin et al. 2017) as well as the *INTErnational Gamma-Ray Astrophysics Laboratory* (*INTEGRAL*; Savchenko et al. 2017a, 2017b) detected a faint 2-s duration GRB (hereafter GRB 170817A), 1.7 s after GW170817 (Abbott et al. 2017c). Although the chance coincidence of finding both transients quasi-contemporaneous and in the same region of the sky is very small, the credible region of the γ-ray localization had a size of ~1100 deg^2 (90% confidence; Blackburn et al. 2017). To firmly establish the connection between GRB 170817A and GW170817 by detecting the afterglow of the GRB in the X-ray and radio bands, numerous groups carried out large follow-up campaigns to very deep limits, but without success (e.g., Alexander et al. 2017a; Bannister et al. 2017; Cenko et al. 2017; Corsi & Kasliwal 2017b; De et al. 2017; Deller et al. 2017; Evans et al. 2017a; Kaplan et al. 2017; Margutti et al. 2017; Resmi et al. 2017; Sugita et al. 2017). It was not until nine days after GW170817 that a brightening X-ray source was detected at the position of AT2017gfo (Troja et al. 2017a). Subsequent X-ray observations confirmed the brightening (Fong et al. 2017; Haggard et al. 2017a). About a week later, Corsi & Kasliwal (2017b) and Mooley et al. (2017) detected an emerging radio source at 3 and 6 GHz as well. While these observations might support the SGRB connection, such a behavior is highly atypical for GRB afterglows (e.g., Piran 2004).

In this Letter, we examine the afterglow properties of AT2017gfo. We present sub-mm and radio observations obtained with the Atacama Large Millimeter/submillimeter Array (ALMA) and the Giant Metrewave Radio Telescope (GMRT) between 1.4 and 44.1 days after the GW detection. We augment our data set with public X-ray, optical, and radio data and confront GRB afterglow models with observations.

---

[23] The luminosity distance was derived for a flat ΛCDM cosmology with $\Omega_m = 0.315$, $\Omega_\Lambda = 0.685$, $H_0 = 67.3$ km s^{-1} Mpc^{-1} (Planck Collaboration XVI 2014). We use this cosmology throughout the paper.

Table 1
Log of Sub-mm/mm and Radio Observations of AT2017gfo

T_{start} (UT)	Epoch (day)	Frequency (GHz)	Integration time (s)	F_ν (μJy)
ALMA				
2017 Aug 18 22:50:40	1.4	338.5	2238	<126
2017 Aug 20 18:19:35	3.2	338.5	2238	<90[a]
2017 Aug 20 22:40:16	3.4	338.5	2238	
2017 Aug 25 22:35:17	8.4	338.5	2238	<150
2017 Aug 26 22:58:41	9.4	338.5	1724	<102
2017 Sep 30 15:22:00	44.1	338.5	1832	<93
GMRT				
2017 Aug 25 09:30:00	7.9	1.39	5400	<69
2017 Sep 09 11:30:00	23.0	1.39	5400	<108
2017 Sep 16 07:30:00	29.8	1.39	5400	<126

Note. The epoch is with respect to the time of GW170817.
[a] The rms was measured after combining both epochs from 2017 August 20.

All uncertainties reported in this Letter are given at 1σ confidence. Non-detections are reported at 3σ confidence, unless stated otherwise.

2. Observations and Data Reduction

We observed the field of AT2017gfo as a part of the observing program 2016.1.00862.T (P.I.: Kim) with ALMA in the Atacama desert (Chile; Wootten & Thompson 2009) and as part of the Director's Discretionary Time (DDT) Proposal DDTB285 with the GMRT, Pune (India; Swarup et al. 1991; P.I.: Resmi).

2.1. ALMA Observations

Our initial ALMA campaign started on 2017 August 18 at 22:50:40 UTC (1.4 days after GW170817) and lasted for eight days (Schulze et al. 2017). In addition, we secured a final epoch ~44 days after GW170817. In total, we obtained six epochs at 338.5 GHz (Table 1). The integration time of each observation was set to reach a nominal rms of ~40 μJy/beam. The initial ALMA observations were performed in the C40-7 configuration, with a field of view of $18''.34$ in diameter and an average synthesized beam of $\approx0''.13 \times 0''.07$. The observation at 44 days after GW170817 was performed in the most extended ALMA configuration, C40-8/9, yielding a synthesized beam of $0''.026 \times 0''.016$.

The ALMA data were reduced with scripts provided by ALMA and with the software package COMMON ASTRONOMY SOFTWARE APPLICATIONS (CASA) version 4.7.2 (McMullin et al. 2007).[24] For each epoch, we created images using TCLEAN, with a pixel size of $0''.01$/px. We interactively selected cleaning regions around detected sources (none corresponding to the AT2017gfo counterpart). The cleaning process was repeated until no clear emission was left. The rms was measured in a $10''$-width box around the central position in the images without primary beam correction.

No significant signal is detected at the position of AT2017gfo. Table 1 summarizes the 3σ detection limits. The galaxy nucleus is well detected and marginally resolved in our data (α, δ (J2000) =

---

[24] https://casa.nrao.edu

$13^{\rm h}09^{\rm m}47{\buildrel{\rm s}\over{.}}69$, $-23°23'02{\buildrel{''}\over{.}}37$). We measure 1.07 ± 0.21 mJy at 338.5 GHz. In addition, we detect a marginally resolved sub-mm galaxy with $F_{338.5\,{\rm GHz}} = 1.15 \pm 0.21$ mJy at α, δ (J2000) = $13^{\rm h}09^{\rm m}48{\buildrel{\rm s}\over{.}}39$, $-23°22'48{\buildrel{''}\over{.}}29$. The quasars J1337−1257 and J1427−4206 were used for band and flux calibration, and J1256 −2547, J1937−3958, and J1258−2219 for phase calibration.

2.2. GMRT Observations

The GMRT is one of the most sensitive low-frequency radio telescopes in operation currently. It operates at low radio frequencies from 150 MHz to 1.4 GHz (Swarup et al. 1991). We secured three epochs in the L band, centered at 1.39 GHz, between 2017 August 25 and 2017 September 16 (i.e., between 7.9 and 29.8 days since GW170817; Table 1; Resmi et al. 2017). The observing time was ∼1.5 hr for each observation. The first epoch was performed with the new 200 MHz correlator that divides the bandpass into 2048 channels, of which ∼70% were usable due to radio frequency interference. The second and the third epoch were performed with the 32 MHz correlator. The synthesized beam sizes were typically $4'' \times 2''$. The quasar 3C286 was used as flux and bandpass calibrator, and J1248−199 was used for phase and additional bandpass calibration. Data reduction was carried out with the NRAO ASTRONOMICAL IMAGE PROCESSING SOFT-WARE[25] (AIPS; Wells 1985) using standard procedures.

While the marginally resolved nucleus of the host galaxy of AT2017gfo, NGC 4993, was detected with ∼570 μJy in 1.39 GHz, no significant signal is detected at the position of AT2017gfo itself. Table 1 summarizes the 3σ detection limits, where the rms level is estimated from source-free regions using the task TVSTAT.

2.3. Other Observations

To augment our data set, we incorporated radio measurements from Corsi & Kasliwal (2017a, 2017b, 2017c), Corsi et al. (2017a, 2017b), Hallinan et al. (2017a), Kaplan et al. (2017), Mooley & Hallinan (2017), Mooley et al. (2017; see also Hallinan et al. 2017b), obtained with the Australia Telescope Compact Array (ATCA) and the Very Large Array (VLA). We used the VLA exposure time calculator[26] to convert the relative measurements of Corsi et al. (2017b) and Mooley et al. (2017) into radio flux densities, adopting rms values 50% higher than nominal to mitigate possible losses due to antennae problems and adverse observing conditions. We also included the X-ray constraints of Evans et al. (2017b), Haggard et al. (2017a), and Troja et al. (2017a) from the *Swift* satellite and *Chandra X-ray Observatory*, as reported in Abbott et al. (2017a), as well as optical photometry obtained with the *Hubble Space Telescope* and ESO's 8.2 m Very Large Telescope (VLT) by Tanvir et al. (2017b).

3. Results and Discussion

3.1. GRB 170817A in the Context of Other SGRBs

The interaction of the GRB blastwave with the circumburst medium produces an afterglow from X-ray to radio frequencies. The peak of the synchrotron afterglow spectrum is, however, expected to be in the sub-mm/mm band and it
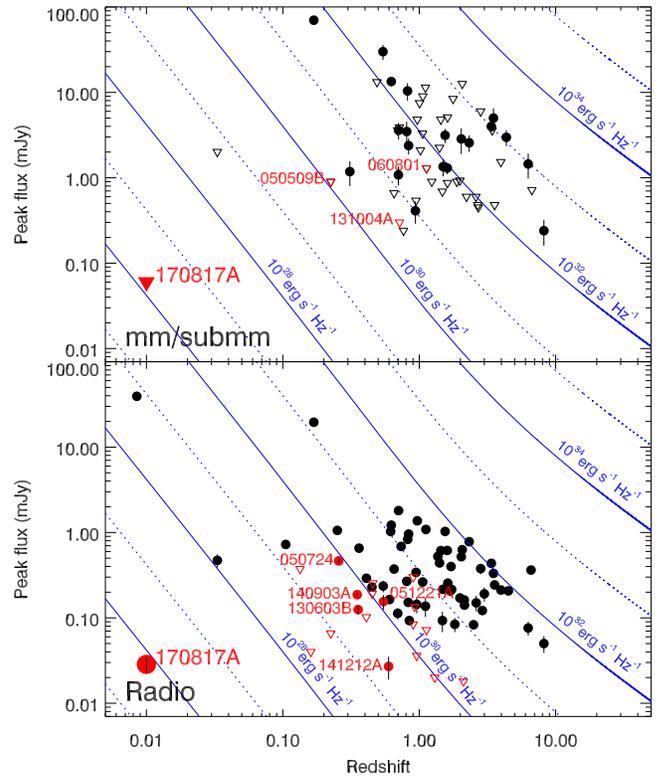

Figure 1. Peak flux densities of GRB afterglows derived from mm/sub-mm (top) and radio (bottom) observations. Filled circles and open triangles denote detections and 3σ limits, respectively. SGRBs are shown in red and LGRBs in black. Solid and dotted blue curves indicate equal afterglow luminosities. The non-detection in the sub-mm corresponds to a luminosity limit of 3×10^{26} erg s^{-1} Hz^{-1}. The faint radio counterpart detected by Corsi et al. (2017b) suggests a peak luminosity of $\sim 7 \times 10^{26}$ erg s^{-1} Hz^{-1}.

rapidly crosses the band toward lower frequencies ($\nu_{\rm m} \propto t^{-3/2}$; Sari et al. 1998). Our initial ALMA 3σ limit of $F_{338.5\,{\rm GHz}} < 126$ μJy at 1.4 days after GW170817 corresponds to a luminosity of 3×10^{26} erg s^{-1} Hz^{-1} at the redshift of AT2017gfo. Comparing this estimate for the peak flux of GRB 170817A to estimates of other GRBs from de Ugarte Postigo et al. (2012; see Figure 1, top panel), our sub-mm afterglow limits are ∼3–4 orders of magnitude fainter than those associated with any long-duration GRBs (LGRBs) or SGRBs.[27]

However, the maximum frequency is also correlated with the energy within the jet and the energy release in γ-rays, e.g., $\nu_m \propto E^{1/2}$ for a constant density circumburst medium (Piran 2004). Abbott et al. (2017c) reported an exceptionally low isotropic-equivalent energy of only $E_{\gamma,{\rm iso}} = (3.08 \pm 0.72) \times 10^{46}$ erg. Hence, it is conceivable that the peak of the afterglow spectrum was already in the radio band during our first ALMA observation. To get an additional estimate of the peak luminosity, we use results in Corsi et al. (2017a). Their measurement of $F_{6\,{\rm GHz}} \sim 28.5$ μ Jy
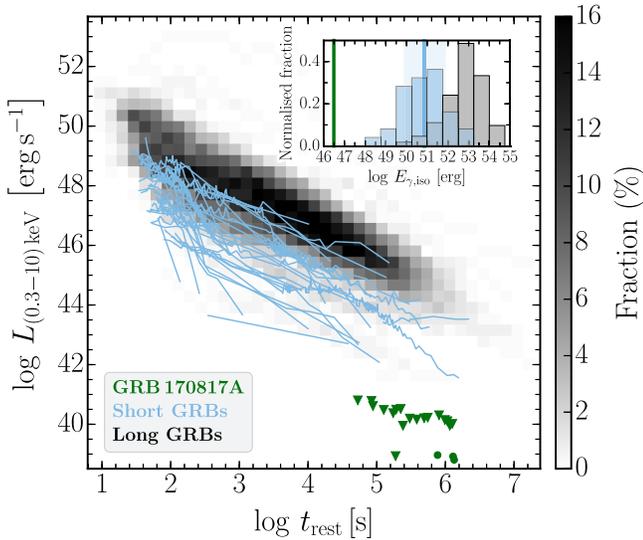

Figure 2. X-ray light curves of GRB afterglows. The parameter space occupied by 402 LGRBs, detected between 2004 December and 2017 September, is indicated by the density plot. Light curves of 31 SGRBs with detected X-ray afterglows are shown in light blue. GRB 170817A lies 2.6 orders of magnitude below the other SGRBs. The inset displays the distribution of energy release at γ-ray energies (SGRBs: blue; LGRBs: gray). The blue vertical line and shaded region indicate the median value and dispersion of the SGRB distribution, respectively.

at 28.5 days after GW170817 translates to a luminosity of $\sim 7 \times 10^{25}\,\mathrm{erg\,s^{-1}\,Hz^{-1}}$. Compared to radio measurements of LGRBs and SGRBs in Fong et al. (2015) and Chandra & Frail (2012), respectively (Figure 1, bottom panel), the radio afterglow is 2 orders of magnitude fainter than those of LGRBs and SGRBs.

While sub-mm and radio observations are direct tracers of the peak of the afterglow spectrum, only $\sim 7\%$ of all *Swift* GRBs were bright enough to attempt sub-mm and radio observations. This observational bias is likely to skew the known population toward the bright end of any luminosity function. On the other hand, almost all of the *Swift* GRBs are detected at X-rays. The mapping between X-ray brightness and the peak of the afterglow spectrum is more complex. It depends on the location of the cooling break, which is usually between the optical and the X-rays, and the density profile of the circumburst medium. Nonetheless, de Ugarte Postigo et al. (2012) showed that X-ray brightness is a useful diagnostic for comparing afterglow luminosities.

To generate an X-ray diagnostic plot, we retrieved the X-ray light curves of 402 LGRBs and 31 SGRBs with detected X-ray afterglows (at least at two epochs) and known redshift from the *Swift* Burst Analyzer (Evans et al. 2010). Identical to Schulze et al. (2014), we computed the rest-frame light curves and resampled the light curves of the LGRB sample on a grid (gray shaded region in Figure 2). The individual light curves of the SGRB sample are shown in light blue. Already the *Swift* non-detections presented in Evans et al. (2017b; downward pointing triangles in Figure 2) revealed that the afterglow is >1.5 dex fainter than the faintest SGRB with detected afterglow (downward pointing triangles in Figure 2). The deep *Chandra* observation by Troja et al. (2017b) at 2.3 days after GW170817 excluded any afterglow brighter than $>10^{39}\,\mathrm{erg\,s^{-1}}$, i.e., a factor of 10 below the *Swift* upper limits.

To put these limits in context, Evans et al. (2017a) placed 10,000 fake GRBs, generated from the flux-limited SGRB sample in D'Avanzo et al. (2014), at the distance of GW170817. These authors estimated that the *Swift* X-ray telescope would have detected $\sim 65\%$ of all simulations. The deeper *Chandra* observations probed a larger portion of the parameter space. However, Rowlinson et al. (2010) showed that a number of SGRBs have extremely rapidly fading X-ray afterglows, which would have evaded detection at the time of the *Swift* and *Chandra* observations.

The new quality of the X-ray emission of AT2017gfo is not only its faintness, but actually its emergence more than a week after GW170817. This behavior is inconsistent with known X-ray afterglows. When the X-ray afterglow was detected with *Chandra* (Haggard et al. 2017b; Margutti et al. 2017; Troja et al. 2017b), the luminosity of $L_{(0.3-10)\mathrm{keV}} \sim 8 \times 10^{38}\,\mathrm{erg\,s^{-1}}$ was still 2.6 dex fainter than that of any GRB *with detected X-ray afterglow*.

This faintness of the afterglow is also reflected in the very low energy release at γ-rays, $E_{\gamma,\mathrm{iso}}$. The observed $E_{\gamma,\mathrm{iso}}$ distribution of SGRBs and LGRBs is shown in the inset of Figure 2. The vertical blue line and the shaded region display the median [$\log(E_\mathrm{iso}/\mathrm{erg}) = 50.88 \pm 0.18$] and the sample dispersion [$\sigma\{\log(E_\mathrm{iso}/\mathrm{erg})\} = 0.99^{+0.14}_{-0.12}$] of the SGRB sample, computed with (PY)MULTINEST (Feroz et al. 2013; Buchner et al. 2014). With a prompt energy release of $3.08 \times 10^{46}\,\mathrm{erg}$ (green vertical line the inset of Figure 2), GRB 170817A was ~ 1.5 dex less energetic than the least energetic SGRB known so far and its deviation from the distribution median is $\sim 4.4\sigma$.

In conclusion, observations of the afterglow revealed an exceptionally under-luminous afterglow at all wavelengths at the position of AT2017gfo. This extremeness is also reflected in the γ-ray properties.

3.2. Modeling the Broadband Afterglow

The previous considerations placed the GRB in the context of LGRBs and SGRBs detected by *Swift*. The discussion neglected the peculiar evolution of the afterglow: non-detection of the afterglow during the first week and its emergence at later epochs. These properties are highly atypical for GRBs, assuming that the GRB jet axis is aligned with our line of sight. In the following, we model the observed evolution from X-rays to radio with templates from two-dimensional relativistic hydrodynamical jet simulations using BOXFIT version 2 with the methods described in van Eerten et al. (2012). The templates are generated from a wide range of physical parameters. Here, we use a nine-parameter model:

$$F_\nu = L(E_{\mathrm{AG,iso}}, n, \theta_{1/2,\mathrm{jet}}, \theta_{\mathrm{obs}}, p, \epsilon_e, \epsilon_B, \xi_N, z)$$

where $E_{\mathrm{AG,iso}}$ is the isotropic-equivalent energy of the blastwave (afterglow),[28] n is the circumburst density at a distance of 10^{17} cm, p is the power-law index of the electron energy distribution, $\theta_{1/2,\mathrm{jet}}$ is the jet half-opening angle, θ_{obs} is the observer/viewing angle, ϵ_e and ϵ_B are the fractions of the internal energy in the shock-generated magnetic field and electrons, respectively, and ξ_N is the fraction of electrons that are accelerated and z is the redshift.

---

[28] In the discussed models, E_iso always corresponds to the isotropic-equivalent energy measured by an on-axis observer.

We fix the fractions of ϵ_e and ξ_N at 0.1 and 1, respectively, and p to 2.43 and the redshift to 0.009854. The other parameters are varied within the following ranges: $\theta_{1/2,\text{jet}} = 5° - 45°$, $E_{\text{AG,iso}} = 10^{47}$–$10^{53}$ erg, $\epsilon_B = 10^{-5}$–10^{-2}, $n = 10^{-4}$–10^{-1} cm^{-3} and $\theta_{\text{obs}} = 0° - 45°$. The afterglow was modeled in a homogeneous ISM environment and we apply this model to eight representative frequencies: 1.4, 3, 6, 21, 338.5 GHz as well as the optical filters $F606W$ and $F475W$ and X-rays at 3 keV.

A critical aspect of the off-axis afterglow modeling is the resolution in azimuthal direction, in particular for models with large θ_{obs} to $\theta_{1/2,\text{jet}}$ ratios. We chose a numerical resolution of 20 and 30, for $\theta_{1/2,\text{jet}} > 9°$ and $\theta_{1/2,\text{jet}} < 9°$, respectively. Comparisons to simulations with a numerical resolution in azimuthal direction of 70 show that the lower-resolution templates accurately capture the temporal evolution of the afterglow, and they are also able to recover the absolute flux scale at maximum to within 20%. The maximum flux of models with very narrow jet are recovered less accurately in off-axis afterglow models. As we show below, these models are not adequate to describe the observed afterglow evolution independent of the issue of the absolute flux scale. The numerical resolution in azimuthal direction was set to unity if the viewing angle is negligible, as suggested by the BOXFIT manual.

The gray curves in Figure 3 display a set of strict on-axis afterglow models (i.e., $\theta_{\text{obs}} = 0$) with a half-opening angle of 5°, $\epsilon_B = 0.01$, $n = 10^{-2}$ cm^{-3}, and for $E_{\text{AG,iso}}$ between 10^{48} and 10^{53} erg. Common to on-axis afterglow models ($\theta_{\text{obs}} < \theta_{1/2,\text{jet}}$) is the strict monotonic decline in X-rays and the optical, whereas the radio can exhibit a plateau or an initial rise. This evolution is in stark contrast to observations of AT2017gfo. The best-matching templates (colored curves in Figure 3) strongly argue for a GRB seen off-axis (i.e., $\theta_{\text{obs}} > \theta_{1/2,\text{jet}}$; possible off-axis LGRB candidates were discussed in Fynbo et al. 2004; Guidorzi et al. 2009; Krühler et al. 2009).

Model 1 (which we call the *wide-jet model*, thin curves in Figure 3) represents an afterglow with an energy reservoir of $\sim 10^{50}$ erg, an energy fraction stored in magnetic fields of $\epsilon_B \sim 10^{-2}$, and a moderately collimated outflow with a half-opening angle of $\theta_{1/2,\text{jet}} \sim 20°$, traversing a circumburst medium with a density of 10^{-2} cm^{-3}. The jet axis and the line of sight are misaligned by 41°. *Model 2* (which we call the *narrow-jet model*, thick curves in Figure 3) represents a more collimated jet with $\theta_{1/2,\text{jet}} \sim 5°$, $E_{\text{AG,iso}} \sim 10^{51}$ erg and $\epsilon_B \sim 2 \times 10^{-3}$, traversing a more tenuous circumburst medium ($n \sim 5 \times 10^{-4}$ cm^{-3}). In this scenario, the line of sight and the GRB jet axis are misaligned by 17°.

The inferred afterglow properties are in both cases very close to the average values of SGRBs in Fong et al. (2015), corroborating that this GRB is *not* different from the population of known SGRBs. The properties of the wide-jet model are consistent with Alexander et al. (2017b), Granot et al. (2017), Margutti et al. (2017), and Troja et al. (2017b). However, the two distinct models, discussed in this Letter, show that there is significant degeneracy between the afterglow parameters (for a more detailed study of the afterglow parameter space, see Granot et al. 2017). More detections are required to better constrain the parameter space. We note that the derived viewing angles for both models are consistent with the conservative limit of $<56°$ from the LIGO signal. Moreover,

the narrow-jet template (*Model 2*) is consistent with the even stricter LIGO limit of $<28°$ (Abbott et al. 2017b).

With the best-match templates in hand, we quantify the contamination of the kilonova by the afterglow. The upper panels in Figure 3 display the light curve in $F475W$ (6.2×10^{12} Hz) and $r'/F606W$ (4.9×10^{12} Hz) by Tanvir et al. (2017b). The contamination by the afterglow in the optical is negligible ($<1\%$) during the week after GW170817 for both models. Hence the inferred KN properties in Tanvir et al. (2017b) do not require any afterglow correction.

3.3. Inferring Jet Parameters from γ-Ray and Afterglow Emission

The observed energy release of a GRB, $E_{\gamma,\text{iso,off}}$, measured by an observer at a viewing angle θ_{obs}, depends on θ_{obs}, $\theta_{1/2,\text{jet}}$, the jet geometry, and the initial bulk Lorentz factor of the jet, Γ_0. Similarly, the observed $E_{\text{peak,off}}$ is a function of the same quantities. The simplest jet model assumes a uniform jet with a negligible surface and predicts that the ratios between $E_{\gamma,\text{iso,off}}$ and on-axis $E_{\gamma,\text{iso}}$, as well as $E_{\text{peak,off}}$ and on-axis E_{peak}, are simple powers of the Doppler factor of the jet (Abbott et al. 2017c; Troja et al. 2017b). However, results already start to change considerably if the finite size of the jet is taken into account (Yamazaki et al. 2003a, 2003b).

In the following, we assume a top-hat jet, similar to Troja et al. (2017b) and Abbott et al. (2017c), but we take into account the finite size of the jet. Donaghy (2006) and Graziani et al. (2005) provided analytical expressions for $E_{\gamma,\text{iso,off}}$ and $E_{\text{peak,off}}$ for such a geometry that also match well the numerical calculations in Yamazaki et al. (2003a, 2003b). In this model, $E_{\gamma,\text{iso,off}}$ and $E_{\text{peak,off}}$ are given by

$$E_{\gamma,\text{iso,off}}$$
$$= \frac{E_{\gamma,\text{iso}}}{2\beta\Gamma_0^4}[f(\beta - \cos\theta_{\text{obs}}) - f(\beta\cos\theta_{1/2,\text{jet}} - \cos\theta_{\text{obs}})],$$

$$E_{\text{peak,off}} = \frac{\langle D(\theta_{\text{obs}})\rangle}{\langle D(\theta_{\text{obs}} = 0)\rangle}E_{\text{peak}},$$

where β the velocity normalized to the speed of light, Γ is the Lorentz factor, the function $f(y)$ is defined as

$$f(y) = \frac{\Gamma_0^2(2\Gamma_0^2 - 1)y^3 + (3\Gamma_0^2\sin^2\theta_{\text{obs}})y + 2\cos\theta_{\text{obs}}\sin^2\theta_{\text{obs}}}{(y^2 + \Gamma_0^{-2}\sin^2\theta_{\text{obs}})^{3/2}},$$

and the average Doppler shift is given by

$$\langle D\rangle = \Gamma_0^{-1}\frac{f(\beta - \cos\theta_{\text{obs}}) - f(\beta\cos\theta_{1/2,\text{jet}} - \cos\theta_{\text{obs}})}{g(\beta - \cos\theta_{\text{obs}}) - g(\beta\cos\theta_{1/2,\text{jet}} - \cos\theta_{\text{obs}})},$$

with

$$g(y) = \frac{2\Gamma^2 y + 2\cos\theta_{\text{obs}}}{(y^2 + \Gamma^{-2}\sin^2\theta_{\text{obs}})^{1/2}}.$$

The equations for $E_{\gamma,\text{iso,off}}$ and $E_{\text{peak,off}}$ depend on the unknown $E_{\gamma,\text{iso}}$, E_{peak} and the initial bulk Lorentz factor Γ_0. Considering the complexity of the expressions, we perform a parameter study. We can limit the possible parameter space by using results from other SGRBs and our afterglow modeling. Cenko et al. (2011) reported that the ratio between $E_{\gamma,\text{iso}}$ and $E_{\text{AG,iso}}$ varies between 0.05 and 40 (mean value being ~ 4). An $E_{\gamma,\text{iso}}$-$E_{\text{AG,iso}}$ ratio of a few has also been observed for SGRBs (Fong et al. 2015). The broadband modeling (Section 3.2)
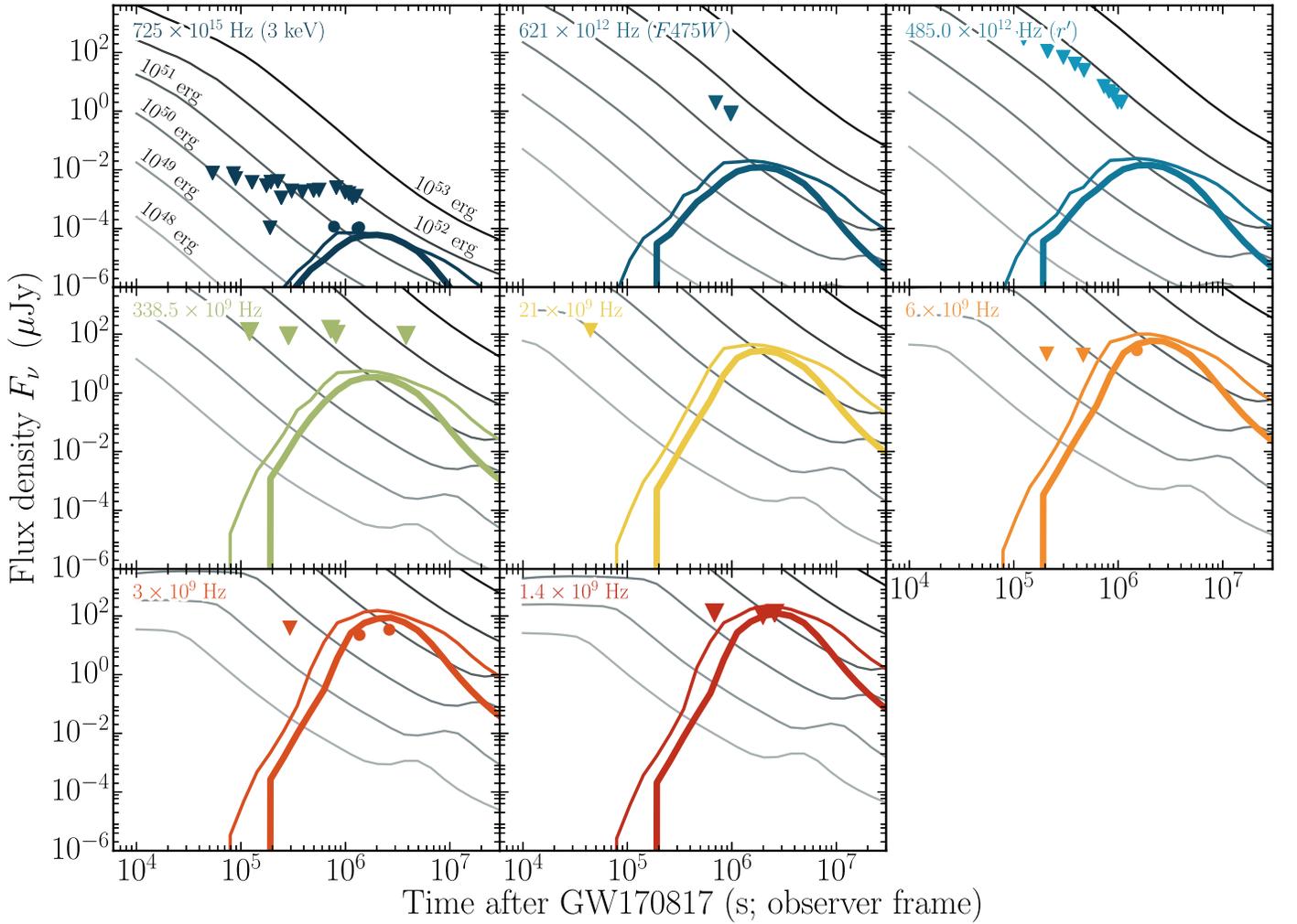
Figure 3. Afterglow from radio to X-ray frequencies (detections: •; non-detections: ▼; our ALMA and GMRT measurements are displayed slightly larger.). The light curves are adequately modeled with two distinct templates: *model 1*—$E_{AG,iso} \sim 10^{50}$ erg, $\theta_{1/2,jet} \sim 20°$, $\theta_{obs} \sim 41°$, $n \sim 10^{-2}$ cm^{-3}, and $\epsilon_B \sim 10^{-2}$ (thin curves); *model 2*—$E_{AG,iso} \sim 10^{51}$ erg, $\theta_{1/2,jet} \sim 5°$, $\theta_{obs} \sim 17°$, $n \sim 5 \times 10^{-4}$ cm^{-3}, and $\epsilon_B \sim 2 \times 10^{-3}$ (thick curves). The gray curves show the evolution of an on-axis afterglow with $\theta_{1/2,jet} = 5°$, $\theta_{obs} = 0°$, $n = 10^{-2}$ cm^{-3}, and $\epsilon_B = 10^{-2}$. The energy in the afterglow was varied between 10^{48} and 10^{53} erg, indicated by the grayscale color pattern. Combining the non-detections at early times and the detections at late-times rules out the entire parameter space of on-axis afterglow models. The rebrightening seen in some on-axis models at $>10^6$ s is due to the contribution of the GRB counter-jet. For a detailed discussion see Section 3.2.

suggests that $E_{AG,iso}$ is between 10^{50} erg and 10^{51} erg, corresponding to $E_{\gamma,iso} = 5 \times 10^{48} - 40 \times 10^{51}$ erg. The E_{peak} distribution of our SGRB comparison sample extends from ~ 40 to ~ 8400 keV (mean peak energy being ~ 490 keV). Goldstein et al. (2017a) reported a peak energy of 185 ± 62 keV for the main emission of GRB 170817A. Hence, we vary E_{peak} between 123 keV and 8400 keV.

In the left and right panels of Figure 4, we display the $E_{\gamma,iso,off}$ and $E_{peak,off}$ as a function of Γ_0. The expected parameter spaces for the two afterglow models are shown in blue (wide-jet) and red (narrow-jet). Overlaid in yellow are the observed $E_{\gamma,iso,off}/E_{peak,iso,off}$ values reported by Goldstein et al. (2017a). The overlapping regions show the allowed parameter space for the GRB, if seen on-axis, for each afterglow model.

The observed span in the $E_{\gamma,iso}$ and $E_{AG,iso}$ allows an initial bulk Lorentz factor between 6 and 40, and 20 and 125 for the wide-jet (*Model 1*) and narrow-jet (*Model 2*), respectively (left panel in Figure 4). However, the highest Lorentz factor would always require $E_{\gamma,iso}/E_{AG,iso} \gtrsim 10$. While such values are not atypical, they are at the upper end of the observed distribution

in Fong et al. (2015). The observed distribution of peak energies of short GRBs narrows the possible parameter space further: $\Gamma_0 < 15$ and $\Gamma_0 < 43$ for *Model 1* and *Model 2*, respectively (right panel in Figure 4), while the required peak energies need to exceed at least several hundred keV. The Lorentz factors are similar to the values in Zou et al. (2017), who assumed a top-jet with negligible surface and used the E_{peak}-$E_{\gamma,iso}$ (derived from SGRBs) and Γ_0-$E_{\gamma,iso}$ (derived from LGRBs) correlations.

To understand these results, we reflect upon the assumptions of this calculation. This parameter study of the jet parameters depends upon the jet half-opening angle, the viewing angle, and the jet geometry. The model in Donaghy (2006) and Graziani et al. (2005) assumes that the γ-ray emission is produced via internal shocks in the GRB jet. According to Graziani et al. (2005), systematic uncertainties may exist between the $E_{peak,off}$ calculated by the above expression and the observed peak of the effective GRB spectrum. Therefore, it may not always be a very accurate representation of the observed E_{peak}. Furthermore, the parameter space is limited to the observed E_{peak} distribution of short GRBs and the
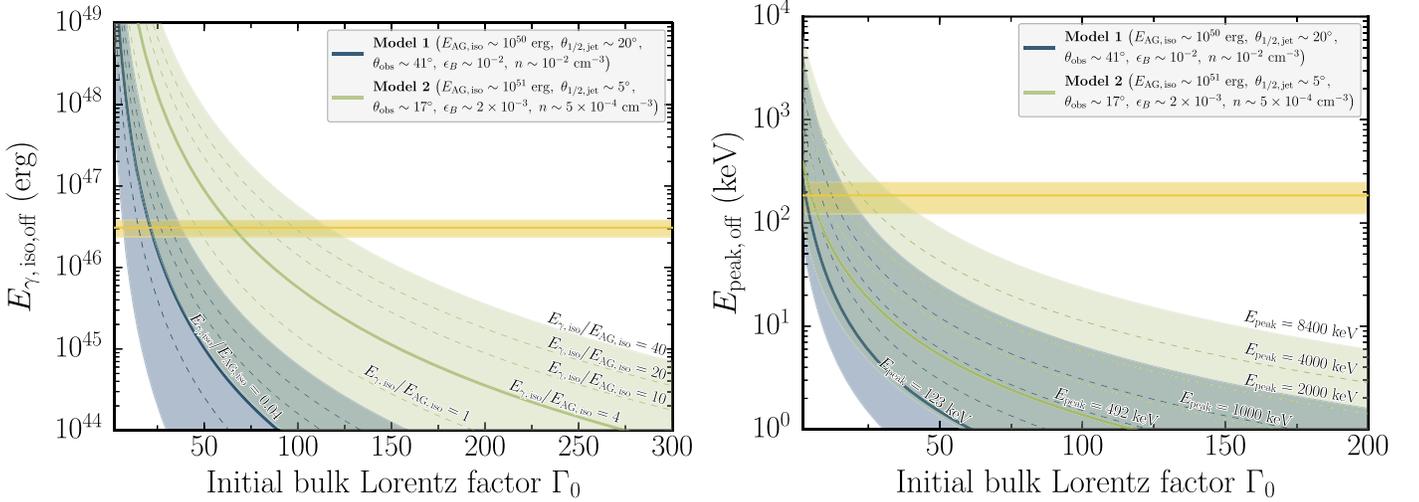
Figure 4. Isotropic γ-ray energy release $E_{\gamma\mathrm{iso,off}}$ and the E_{peak} of the prompt emission measured by an off-axis observer, as a function of Γ_0. We use the model in Donaghy (2006) to predict the allowed loci of the parameter spaces for GRB 170817A. The loci depend on the jet geometry and the viewing angle that we obtained from the broadband modeling in Section 3.2. The known distributions for $E_{\gamma,\mathrm{iso}}/E_{\mathrm{AG,iso}}$ (Cenko et al. 2011), as well as the observed peak energy distribution of our SGRB comparison sample, further limit the possible parameter space to the shaded regions (*Model 1*: blue; *Model 2*: red). Curves of particular values are displayed by the dashed curves. The solid curves indicates the location of the distribution mean values. The parameter space is furthermore limited by the results from *Fermi* reported in Goldstein et al. (2017a), displayed in yellow. The bands encompassing the *Fermi* measurements indicate the 1σ confidence intervals. These constraints limit Γ_0 to <15 and <43 for *Model 1* and *Model 2*, respectively.

known ratios between $E_{\gamma,\mathrm{iso}}$ and $E_{\mathrm{AG,iso}}$, and the parameters of GRB170817 as measured by *Fermi*.

Our broadband modeling is based on a small number of detections and we showed that there is substantial degeneracy in the model parameters. This degeneracy is also visible in the Γ_0–$E_{\gamma,\mathrm{iso,off}}$ and the Γ_0–$E_{\mathrm{peak,off}}$ parameter spaces (Figure 4). A more sophisticated afterglow modeling and the inclusion of more afterglow observations can reduce the degeneracy. The conclusions of this analysis also depend significantly on the observed γ-ray properties of GRB 170817A. Goldstein et al. (2017b) reported an error of 33% on the peak energy. A substantially lower peak energy would allow higher Γ_0 for lower peak energies (for an independent analysis of the *Fermi*-GBM data, see Zhang et al. 2017).

3.4. Low-frequency Radio Emission from Merger Ejecta

Non-relativistic shocks from the merger ejecta are thought to emit at radio frequencies (Nakar & Piran 2011). This model predicts that the emission peaks in the MHz regime and at the epoch of deceleration of the non-relativistic shock, which is expected to be on the order of months to years after the merger.

To examine whether this mechanism could produce a bright transient months after GW170817, we use the observed properties of the kilonova and the afterglow. The expected brightness at optically thin GHz frequencies would be

$$f_\nu(t) = 655\,\mathrm{mJy}\; n_0^{1.8} \frac{R(t)^3}{10^{17}} \beta(t)^{3.75} \epsilon_B^{0.78} \epsilon_e \left(\frac{\nu}{\mathrm{GHz}}\right)^{-0.55},$$

for an electron index of 2.1, where $R(t)$ is the radius of the shock front (normalized to 10^{17} cm), and $\beta(t)$ is the velocity normalized to the speed of light c. This expression is derived from the peak synchrotron flux and the characteristic synchrotron frequency ν_m of the power-law electron distribution, and is in agreement with expressions in Nakar & Piran (2011). The radius and the observed time t are related through $R(t) = \beta ct$. The epoch of deceleration, where

the swept-up mass equals the ejected mass, is given by $t_{\mathrm{dec}} = 7\,\mathrm{yr}\left(\frac{M_{\mathrm{ej,\odot}}}{n_0}\right)^{1/3}\beta_0^{-1}$, where β_0 is the normalized initial velocity.

Tanvir et al. (2017b) concluded that the merger ejected $\sim 5 \times 10^{-4}\,M_\odot$ with a velocity of $0.1\,c$. Along with a circumburst medium density, $n = 0.01$ cm^{-3}, we estimate the brightness at 1.4 GHz to be $\sim 60\,\mu$Jy for a deceleration timescale of 55 years. A smaller ambient density will further reduce the flux and increase the t_{dec}.

Considering the results of Smartt et al. (2017), where a higher ejected mass of $0.01 M_\odot$ was estimated to be released with a similar β, the deceleration time will be ~ 70 years, and the observed flux will remain the same as it is insensitive to M_{ej}. Therefore, the outlook, assuming this model is valid, is bleak.

The merger remnant, if a magnetar, can inject additional energy into the shock (Metzger & Bower 2014). This increased energy will also delay t_{dec}. In this model, from the observed $\beta = 0.1$ and best-fit ambient density $n_0 = 0.01$ cm^{-3}, $t_{\mathrm{dec}} = 260\, E_{\mathrm{mag,52}}$ years, where $E_{\mathrm{mag,52}}$ is the energy input from the magnetar. The peak flux in 1.4 GHz at $t_{\mathrm{dec}} \sim 3$ mJy for our parameters, which, as in the previous case, scales down as a t^3 power-law to the current epoch. Therefore, we do not expect any detectable emission at GMRT frequencies at present from the merger ejecta, consistent with our observations.

4. Summary

LIGO/Virgo detected a BNSM at a distance of $\sim$44 Mpc on 2017 August 17. Rapid optical and near-IR follow-up observations detected a new transient, AT2017gfo, in the credible region of GW170817 with properties consistent with KN models. Gamma-ray satellites detected the short GRB 170817A quasi-contemporaneously with GW170817, but owing to the poor localization at γ-rays this did not exclude a chance alignment.

We observed the position of AT2017gfo with ALMA and GMRT at 338.5 and 1.4 GHz, respectively, from 1.4 days to 44 days after the merger, our objective being to constrain the GRB afterglow component. The afterglow evaded detection at all epochs. Our radio and sub-mm observations allow us to place a firm upper limit of a few 10^{26} erg s^{-1} in the sub-mm and radio, probing a regime $>$2–4 orders of magnitudes fainter than previous limits on SGRBs.

The emergence of an X-ray and radio transient at the position of AT2017gfo at 9 and 17 days after GW170817, respectively, is highly atypical for GRBs. Modeling the evolution from radio to X-ray frequencies with templates generated from 2D relativistic hydrodynamical jet simulations excludes all on-axis afterglow models ($\theta_{1/2,\mathrm{jet}} > \theta_{\mathrm{obs}}$) with sensible physical parameters. Adequate models, describing the evolution from X-ray to radio frequencies, require strict off-axis afterglow templates where $\theta_{1/2,\mathrm{jet}} < \theta_{\mathrm{obs}}$. *Model 1* favors a jet, powered by $E_{\mathrm{AG,iso}} \sim 10^{50}$ erg, with magnetic equipartition of $\epsilon_B \sim 10^{-2}$ and an initial half-opening angle of $\sim 20°$, traversing a circumburst medium with $n = 10^{-2}$ cm^{-3}. The second model suggests a more collimated jet: $E_{\mathrm{AG,iso}} \sim 10^{51}$ erg, $\theta_{1/2,\mathrm{jet}} \sim 5°$, $\epsilon_B = 2 \times 10^{-3}$, $n = 5 \times 10^{-4}$ cm^{-3}. More detections of the afterglow are needed to reduce the degeneracy in the model parameters. In both cases, our line of sight and the GRB jet axis were misaligned by $\sim 41°$ (wide-jet model) and $\sim 20°$ (narrow-jet model), explaining the emergence of the afterglow only a week after the GRB. The viewing angle measurements are consistent with upper limits by Abbott et al. (2017b).

The jet parameters are, in both cases, consistent with mean values of the *Swift* SGRB population. Using $\theta_{1/2,\mathrm{jet}}$, θ_{obs}, and $E_{\mathrm{AG,iso}}$ of the blastwave, we inferred the true γ-ray energy release and initial bulk Lorentz factor (Γ_0) of the flow. We find evidence for an ultra-relativistic jet with $\Gamma_0 < 15/ < 43$ for *Model 1/2*. The prompt energy release has to be at least a factor of a few higher than the kinetic energy in the afterglow, and peak energies of least several hundred keV that an on-axis observer would have recorded. Therefore, we conclude that a uniform top-hat jet model can broadly explain the observed gamma-ray properties of GRB 170817A. Limiting this parameter study is the degeneracy in the afterglow parameters, due to the limited amount of data, and the large uncertainties of the observed peak energy.

Using the best-match template we assessed if the afterglow contaminated significantly the KN optical emission. The contamination is $<$1% during the first week after GW170817. We also calculated the expected radio emission from the merger ejecta and found it to be negligible presently.

The afterglow modeling allows us to draw the following conclusions: (i) this is the first robust detection of an off-axis GRB with $\theta_{\mathrm{obs}} > \theta_{1/2,\mathrm{jet}}$ and (ii) AT2017gfo and GRB 170817A have the same progenitor. These findings, in conjunction with the spectroscopic evidence for *r*-process elements in spectra of AT2017gfo (e.g., Pian et al. 2017; Smartt et al. 2017), demonstrate that some SGRBs are connected with BNSMs and firmly establishes that AT2017gfo and GRB 170817A are the electromagnetic counterpart to GW170817.

ORCID iDs

S. Kim ⓘ https://orcid.org/0000-0001-8332-0023
J. González-López ⓘ https://orcid.org/0000-0003-3926-1411
F. E. Bauer ⓘ https://orcid.org/0000-0002-8686-8737
N. R. Tanvir ⓘ https://orcid.org/0000-0003-3274-6336
S. Covino ⓘ https://orcid.org/0000-0001-9078-5507
J. P. U. Fynbo ⓘ https://orcid.org/0000-0002-8149-8298
J. Hjorth ⓘ https://orcid.org/0000-0002-4571-2306
D. Malesani ⓘ https://orcid.org/0000-0002-7517-326X
B. Milvang-Jensen ⓘ https://orcid.org/0000-0002-2281-2785
R. Sánchez-Ramírez ⓘ https://orcid.org/0000-0002-7158-5099
D. J. Watson ⓘ https://orcid.org/0000-0002-4465-8264
K. Wiersema ⓘ https://orcid.org/0000-0002-9133-7957

References

Abadie, J., Abbott, B. P., Abbott, R., et al. 2010, CQGra, 27, 173001
Abbott, B. P., Abbott, R., Abbott, T. D., et al. 2016, PhRvL, 116, 241102
Abbott, B. P., Abbott, R., Abbott, T. D., et al. 2017a, ApJL, 848, L12
Abbott, B. P., Abbott, R., Abbott, T. D., et al. 2017b, PhRvL, 119, 161101
Abbott, B. P., Abbott, R., Abbott, T. D., et al. 2017c, ApJL, 848, L13
Alexander, K., Berger, E., Fong, W., et al. 2017b, ApJL, 848, L21
Alexander, K., Fong, W., & Berger, E. 2017a, GCN, 21589
Allam, S., Annis, J., Berger, B., et al. 2017, GCN, 21530
Bannister, K., Lynch, C., Kaplan, D., & Murphy, T. 2017, GCN, 21537
Berger, E. 2014, ARA&A, 52, 43
Blackburn, L., Briggs, N. S., Broida, J., et al. 2017, GCN, 21506
Bromberg, O., Nakar, E., Piran, T., & Sari, R. 2013, ApJ, 764, 179
Buchner, J., Georgakakis, A., Nandra, K., et al. 2014, A&A, 564, A125
Cenko, S. B., Emery, S. W. K., Campana, S., et al. 2017, GCN, 21572
Cenko, S. B., Frail, D. A., Harrison, F. A., et al. 2011, ApJ, 732, 29
Chandra, P., & Frail, D. A. 2012, ApJ, 746, 156
Corsi, A., Hallinan, G., Mooley, K., et al. 2017a, GCN, 21815
Corsi, A., Kasliwal, M. M., Frail, D., & Paliyaguru, N. T. 2017b, GCN, 201664
Corsi, A., & Kasliwal, M. M. 2017a, GCN, 21613
Corsi, A., & Kasliwal, M. M. 2017b, GCN, 21614
Corsi, A., & Kasliwal, M. M. 2017c, GCN, 21636
Coulter, D. A., Kilpatrick, C. D., Siebert, M. R., et al. 2017a, GCN, 21529
Coulter, D. A., Kilpatrick, C. D., Siebert, M. R., et al. 2017b, TNS
    Astronomical Transient Report, 13195
D'Avanzo, P., Salvaterra, R., Bernardini, M. G., et al. 2014, MNRAS,
    442, 2342
De, K., Mooley, K., Chandra, P., et al. 2017, GCN, 21708
de Ugarte Postigo, A., Lundgren, A., Martín, S., et al. 2012, A&A, 538, A44
Deller, A., Bailes, M., Andreoni, I., et al. 2017, GCN, 21588
Donaghy, T. Q. 2006, ApJ, 645, 436
Eichler, D., Livio, M., Piran, T., & Schramm, D. N. 1989, Natur, 340, 126
Einstein, A. 1918, Sitzungsberichte der Königlich Preußischen Akademie der
    Wissenschaften (Berlin), 154
Einstein, A. 1916, Sitzungsberichte der Königlich Preußischen Akademie der
    Wissenschaften (Berlin), 688
Evans, P. A., Cenko, S. B., Kennea, J. A., et al. 2017b, Sci, https://doi.org/
    10.1126/science.aap9580
Evans, P. A., Kennea, J., Breeveld, A. A., et al. 2017a, GCN, 21550
Evans, P. A., Willingale, R., Osborne, J. P., et al. 2010, A&A, 519, A102
Feroz, F., Hobson, M. P., Cameron, E., & Pettitt, A. N. 2013, arXiv:1306.2144
Fong, W., Berger, E., Margutti, R., & Zauderer, B. A. 2015, ApJ, 815, 102
Fong, W., Margutti, R., & Haggard, D. 2017, GCN, 21786
Fynbo, J. P. U., Sollerman, J., Hjorth, J., et al. 2004, ApJ, 609, 962
Goldstein, A., Veres, P., von Kienlin, A., et al. 2017a, GCN, 21528
Goldstein, A., Veres, P., Burns, E., et al. 2017b, ApJL, 848, L14
Granot, J., Gill, R., Guetta, D., & De Colle, F. 2017, MNRAS, submitted
    (arXiv:1710.06421)
Graziani, C., Lamb, D. Q., & Donaghy, T. Q. 2005, BAAS, 37, 507
Guidorzi, C., Clemens, C., Kobayashi, S., et al. 2009, A&A, 499, 439
Haggard, D., Nynka, M., Kalogera, V., et al. 2017a, GCN, 21798
Haggard, D., Nynka, M., Ruan, J. J., et al. 2017b, ApJL, 848, L31
Hallinan, G., Corsi, C., Mooley, K., Frail, D. A., & Kasliwal, M. 2017a, GCN,
    21929
Hallinan, G., Corsi, A., Mooley, K. P., et al. 2017b, Sci, https://doi.org/
    10.1126/science.aap9855
Hjorth, J., Levan, A. J., Tanvir, N. R., et al. 2017, ApJL, 848, L31
Jin, Z.-P., Hotokezaka, K., Li, X., et al. 2016, NatCo, 7, 12898
Jin, Z.-P., Li, X., Cano, Z., et al. 2015, ApJL, 811, L22
Kann, D. A., Klose, S., Zhang, B., et al. 2011, ApJ, 734, 96
Kaplan, D., Murphy, T., Bannister, K., et al. 2017, GCN, 21574
Kasen, D., Badnell, N. R., & Barnes, J. 2013, ApJ, 774, 25
Krühler, T., Greiner, J., Afonso, P., et al. 2009, A&A, 508, 593
Levan, A. J., Lyman, J. D., Tanvir, N. R., et al. 2017, ApJL, 848, L28
Li, L.-X., & Paczyński, B. 1998, ApJL, 507, L59
Margutti, R., Berger, E., Fong, W., et al. 2017, ApJL, 848, L20
McMullin, J. P., Waters, B., Schiebel, D., Young, W., & Golap, K. 2007, in
    ASP Conf. Ser. 376, Astronomical Data Analysis Software and Systems
    XVI, ed. R. A. Shaw, F. Hill, & D. J. Bell (San Francisco, CA: ASP), 127
Melandri, A., Campana, S., Covino, S., et al. 2017, GCN, 21532
Metzger, B. D. 2017, LRR, 20, 3
Metzger, B. D., & Bower, G. C. 2014, MNRAS, 437, 1821
Mooley, K. P., & Hallinan, G. 2017, GCN, 21650
Mooley, K. P., Hallinan, G., & Corsi, A. 2017, GCN, 21814
Nakar, E. 2007, PhR, 442, 166
Nakar, E., & Piran, T. 2011, Natur, 478, 82
Pian, E., D'Avanzo, P., Benetti, S., et al. 2017, Natur, 551, 67
Piran, T. 2004, RvMP, 76, 1143
Planck Collaboration XVI 2014 A&A, 571, A16
Resmi, L., Misra, M., Tanvir, N. R., O'Brian, P., & Schulze, S. 2017, GCN, 21768
Rosswog, S. 2005, ApJ, 634, 1202
Rowlinson, A., O'Brien, P. T., Tanvir, N. R., et al. 2010, MNRAS, 409, 531
Sari, R., Piran, T., & Narayan, R. 1998, ApJL, 497, L17
Savchenko, V., Ferrigno, C., Kuulkers, E., et al. 2017b, ApJL, 848, L15
Savchenko, V., Mereghetti, S., Ferrigno, C., et al. 2017a, GCN, 21507
Schulze, S., Malesani, D., Cucchiara, A., et al. 2014, A&A, 566, A102
Schulze, S., Malesani, D., Cucchiara, A., et al. 2017, GCN, 21747
Siebert, M. R., Foley, R. J., Drout, M. R., et al. 2017, ApJL, 848, L26
Smartt, S. J., Chen, T.-W., Jerkstrand, A., et al. 2017, Natur, 551, 75
Sugita, S., Kawai, N., Serino, M., et al. 2017, GCN, 21555
Swarup, G., Ananthakrishnan, S., Kapahi, V. K., et al. 1991, CSci, 60, 95
Tanaka, M., Hotokezaka, K., Kyutoku, K., et al. 2014, ApJ, 780, 31
Tanvir, N. R., & Levan, A. J. 2017a, GCN, 21544
Tanvir, N. R., Levan, A. J., Fruchter, A. S., et al. 2013, Natur, 500, 547
Tanvir, N. R., Levan, A. J., Gonzalez-Fernandez, C., et al. 2017b, ApJL,
    848, L27
Troja, E., Piro, L., Sakamoto, T., et al. 2017a, GCN, 21765
Troja, E., Piro, L., van Eerten, H., et al. 2017b, Natur, 551, 71
van Eerten, H., van der Horst, A., & MacFadyen, A. 2012, ApJ, 749, 44
von Kienlin, A., Meegan, C., & Goldstein, A. 2017, GCN, 21520
Wells, D. C. 1985, in Data Analysis in Astronomy, ed. V. di Gesu et al. (New
    York: Plenum), 195
Wootten, A., & Thompson, A. R. 2009, IEEEP, 97, 1463
Yamazaki, R., Ioka, K., & Nakamura, T. 2003a, ApJ, 593, 941
Yamazaki, R., Yonetoku, D., & Nakamura, T. 2003b, ApJL, 594, L79
Yang, S., Valenti, S., Sand, D., et al. 2017, GCN, 21531
Zhang, B., Zhang, B.-B., Virgili, F. J., et al. 2009, ApJ, 703, 1696
Zhang, B.-B., Zhang, B., Sun, H., et al. 2017, arXiv:1710.05851
Zou, Y.-C., Wang, F.-F., Moharana, R., et al. 2017, arXiv:1710.07436